ACS Combinatorial Science

Research Article

pubs.acs.org/acscombsci

Combinatorial Synthesis of Cu/$(Ta_xNb_{1-x})_2O_5$ Stack Structure for Nanoionics-Type ReRAM Device

Takahiro Nagata,* Masamitsu Haemori, and Toyohiro Chikyow

International Center for Materials Nanoarchitectonics (WPI-MANA), National Institute for Materials Science, 1-1 Namiki, Tsukuba 305-0044, Japan

ABSTRACT: Resistive random access memory (ReRAM) has been proposed as a new application for oxide materials. We have proposed a Cu electrode/dielectric oxide/bottom electrode stack structure as a potential ReRAM material that is compatible with the LSI process. Control of the switching voltage and the initial conductive filament formation process is beneficial for actual applications. To control the switching property by controlling the valence state of metals, we investigated the Ta−Nb binary oxide ($(Ta_xNb_{1-x})_2O_5$) system as a dielectric oxide layer using a combinatorial method. A combinatorial pulsed laser deposition method was used to fabricate the $(Ta_xNb_{1-x})_2O_5$ system systematically on a Pt/Si substrate. X-ray photoelectron spectroscopy revealed defect formation relating to Ta and the compensation of oxygen vacancies caused by a change in the valence number of Nb. As the Ta content decreased, there were a decrease in the threshold voltage of the low resistive state and an enhancement of the leakage current, meaning that the switching properties can be controlled by controlling the $(Ta_xNb_{1-x})_2O_5$ system.

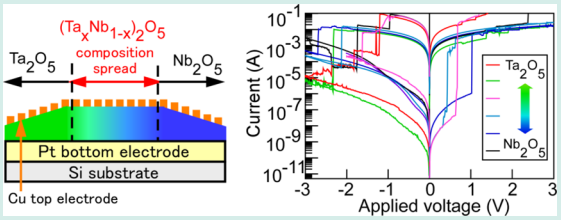

KEYWORDS: *resistive random access memory, dielectric oxide, X-ray photoelectron spectroscopy, combinatorial pulsed laser deposition method*

INTRODUCTION

Resistive random access memory (ReRAM) based on resistive switching phenomena has attracted a great deal of attention for next-generation nonvolatile memory applications.[1,2] Many kinds of material combinations and structures have been proposed for ReRAM applications. A typical resistive switching model is based on a thermal effect initiated by a voltage-induced partial dielectric breakdown that forms a discharge filament modified by Joule heating.[3,4] The intrinsic material properties also induce changes in resistance. For example, the insulator−metal transition in perovskite oxides, such as $(Pr,Ca)MnO_3$[5−7] and $SrTiO_3$:Cr[8] is induced by electronic charge injection operations such as doping. In our research, we focus on the nanoionics model,[9] whose resistive change is based on electrode reactions in solid electrolytes. This model was originally demonstrated by using chalcogenide materials, such as AgS and Cu_2S.[10−12] The fundamental unit cell is composed of a solid electrolyte sandwiched between two conductive electrodes, which are generally Ag or Cu and Pt. A bias application ionizes the solid electrolyte and causes the ions to migrate, resulting in the formation of a conducting path between the two electrodes. The noteworthy electrical characteristics of these devices are the bipolar behavior controlled by the polarity of the applied voltage and their two different (high and low) resistance states. However, as regards a practical large-scale integration (LSI) process and its application, chalcogenide materials are incompatible with the current LSI process owing to their higher vapor pressure, and in the fact that they contaminate the equipment. To overcome these problems, an oxide-based ReRAM with the nanoionics model has been proposed as a new application for oxides.[13−17] We also investigated suitable electrode and matrix materials for the LSI process, and demonstrated the resistance switching behavior of the Cu/HfO_2/Pt system.[18−20] There has been increased interest in the use of high-k dielectric oxides as potential ReRAM materials. Moreover, switching voltage control is beneficial for actual applications. In terms of controlling the operating voltage, the matrix materials are critical for controlling the diffusion of Cu. Metal ions diffuse in a solid electrolyte through defects or grain boundaries, and an electrochemical reaction at another electrode, meaning that the matrix materials should affect the switching voltage.

In this study, to control the metal ion diffusion properties induced by the oxygen vacancy and the valence of metals, we investigated the Ta−Nb binary oxide $(Ta_xNb_{1-x})_2O_5$ system using a combinatorial method. Both oxides are candidate high-k materials and have high affinity with the LSI process. The physical properties of Ta and Nb are similar as regards ion radius, electronegativity, and oxidation number although they differ in terms of Gibbs free energy for oxidization (ΔG). On the basis of the Ellingham diagram, tantalum oxide (TaO_x) typically has two different valence states with the following ΔG values at room temperature; Ta_2O_5 (Ta^{5+}) $\Delta G = -760.5$ kJ mol^{-1} and TaO (Ta^{2+}) $\Delta G = -54.125$ kJ mol^{-1}.[21] In contrast, niobium oxide (NbO_x) typically has three different valence states with the following ΔG values at room temperature; Nb_2O_5 (Nb^{5+}) $\Delta G = -704.8$ kJ mol^{-1}, NbO_2 (Nb^{4+}) $\Delta G = -733.5$ kJ mol^{-1}, and NbO

Received: April 2, 2013
Revised: June 28, 2013
Published: July 24, 2013

(Nb^{2+}) $\Delta G = -773.3$ kJ mol^{-1}. These energy differences can be expected to induce a gradient in the ion diffusion properties of the $(Ta_xNb_{1-x})_2O_5$ system.

EXPERIMENTAL PROCEDURES

A 100-nm-thick Pt bottom electrode layer was deposited on a Si substrate by DC sputtering at room temperature. A Ta–Nb binary oxide film was deposited on the Pt bottom electrode by combinatorial pulsed laser deposition (combi-PLD) using similar procedures to the previously reported binary film deposition as shown in Figure 1a.[22,23] A composition-spread

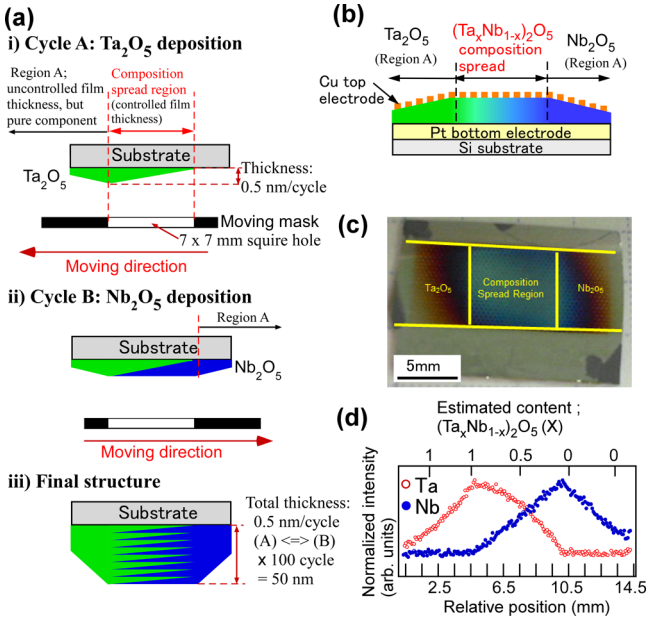

Figure 1. (a) Schematic illustration of composition spread thin film sample fablication procedures, a composition-spread deposition cycle. There were two steps: (i) Ta_2O_5 deposition and (ii) Nb_2O_5 deposition. In each deposition, a mask moved at constant speed from one side of the substrate to the other, after which the targets was changed. Alternating between steps (i) and (ii) created composition-spread samples with film thickness of 50 nm (iii). (b) Schematic illustration, (c) photographic image, and (d) composition mapping measured by XRF of Cu/$(Ta_xNb_{1-x})_2O_5$/Pt structure.

deposition cycle was consisted of two steps. In each one, a mask with a 7 mm squire shaped hole moved at constant speed from one side of the substrate to the other by 6 mm, after which the targets was changed. The maximum film thickness in one cycle was 0.5 nm. Alternating between steps (i) and (ii) created composition-spread region with a width of 8 mm (iii). The film thickness in the composition spread region was a constant 50 nm. The film thickness in the Ta_2O_5 and Nb_2O_5 regions other than the composition-spread region mentioned as "Region A" in Figure 1 exhibited a constant decrease from center to edge, which is unintentionally fabricated due to the hole shape of the mask. The pulse repetition rate of the KrF excimer laser (Coherent, COMPexPro 102, λ = 248 nm) was 5 Hz and the laser energy density was approximately 1.5 J/cm^2. During the deposition, the substrate temperature was maintained at 300 °C. The oxygen partial pressure was kept at 1×10^{-4} Torr. Figure 1b shows a sample structure. For current–voltage (I–V) measurements, 200-nm-thick Cu circular top contacts 100 μm in diameter were deposited by using a metal contact mask and DC sputtering at room temperature. The metal composition and the surface morphology were characterized with an X-ray fluorescence spectrometer (XRF: Shimadzu, μEDX-1400) and atomic force microscopy (AFM: SII, SPI-4000 with E-sweep). The crystal structure was identified by X-ray diffraction (XRD). An XRD system equipped with a 5 kW rotating anode Cu target and a high-resolution 2D-detector (BRUKER AXS, D8 Discover Super Speed with GADDS) was used to determine the phases and structure. The 2D-detector system can detect part of the Debye–Scherrer ring rapidly and two-dimensionally. The I–V measurements were performed with a semiconductor parameter analyzer (Agilent, B1500) at room temperature. A positive bias was applied to the top Cu electrode and the Pt electrode was grounded. The chemical bonding state was evaluated by X-ray photoelectron spectroscopy (XPS: Thermo Scientific, VG Theta Probe) using monochromated Al Kα X-rays at an energy of 1486.6 eV. The total energy resolution of the XPS was 700 meV. To eliminate charging up effects, the sample was neutralized with a charge neutralizer and grounded to the system, whose energy coincides with the Fermi level position of Au, by a conductive Cu tape. The XPS data were calibrated against the Au $4f_{7/2}$ peak (84.0 eV) and the Fermi level position of Au.

RESULTS AND DISCUSSION

Figure 1c and d show a sample photographic image and results of metal composition measurements by XRF, respectively. In Figure 1c, the yellow lines indicate the composition spread region. The XRF measurements revealed that the Ta and Nb content changes continuously, suggesting that composition spread samples were obtained.

Figure 2a shows 2D-XRD images of the Ta_2O_5 and Nb_2O_5 regions. Ring patterns at 39.8° and 46.2° correspond to the Pt

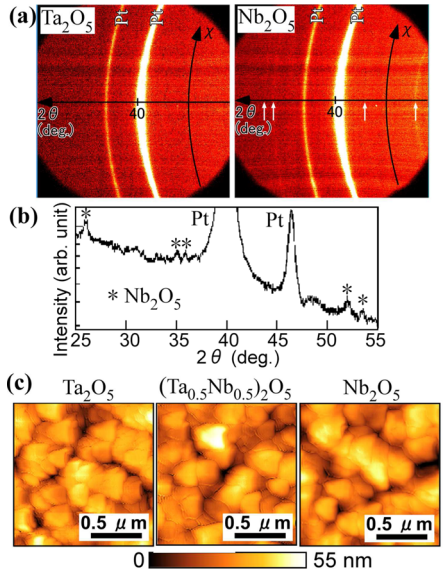

Figure 2. (a) 2D-XRD image of Ta_2O_5 and Nb_2O_5 regions, (b) 2θ–ω plot of Nb_2O_5 region, and (c) AFM images of Nb_2O_5, $(Ta_{0.5}Nb_{0.5})_2O_5$, and Ta_2O_5 regions.

bottom electrode. The Ta_2O_5 region exhibited no diffraction pattern, indicating an amorphous structure. With the Nb_2O_5 region, the 2D-XRD image showed additional weak ring patterns, which are indicated by white arrows in Figure 2a and confirmed as Nb_2O_5 structure by a 2θ–ω plot as shown in Figure 2b. These result revealed that the region included a small polycrystalline phase. The other Ta–Nb binary regions showed the same 2D-

dx.doi.org/10.1021/co4000425 | ACS Comb. Sci. 2013, 15, 435–438

XRD patterns as the Ta_2O_5 region (not shown). Figure 2c shows AFM images of the Ta_2O_5, $(Ta_{0.5}Nb_{0.5})_2O_5$, and Nb_2O_5 regions. The surface morphology also indicated that the thin film consisted of fine 200-nm grains. The obtained root-mean-square (RMS) roughness was 7 nm. The $(Ta_xNb_{1-x})_2O_5$ regions also had a similar grained structure. The AFM observation and XRD characterization revealed that the thin films had many grain boundaries. This as-deposited Ta −Nb binary oxide film with a grained structure was used for XPS and I−V measurements.

XPS measurements were performed to investigate the valence state of the metals and the chemical bonding state of oxygen. Figure 3a shows XPS intensity mapping for Nb 3d, O 1s, and Ta

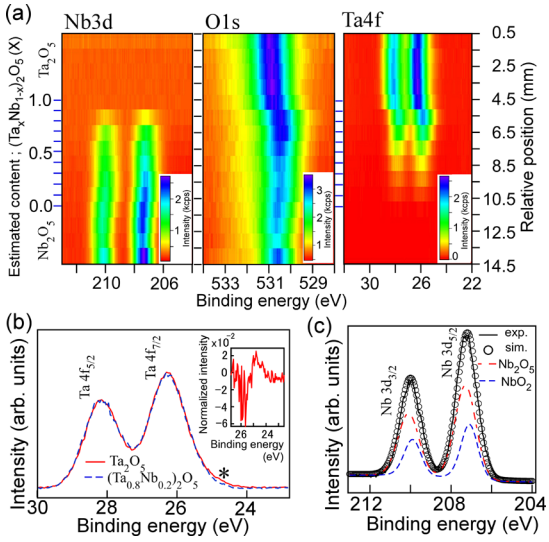

Figure 3. (a) XPS mapping images for Nb 3d, O 1s, and Ta 4f core level spectra. (b) XPS for Ta 4f of Ta_2O_5 (solid line), and $(Ta_{0.8}Nb_{0.2})_2O_5$ (dashed line). To compare the spectrum shape, the spectrum of $(Ta_{0.8}Nb_{0.2})_2O_5$ were shifted by 0.5 eV. The inset shows the difference peak, which is the Ta 4f peak of Ta_2O_5 minus that of $(Ta_{0.8}Nb_{0.2})_2O_5$. (c) XPS for Nb 3d of $(Ta_{0.2}Nb_{0.5})_2O_5$. The solid lines and open circles show the experimental spectrum and sum-fitted curve, respectively. The dashed lines are fitted curves for each bond: Nb_2O_5 and NbO_2.

4f core level spectra. In the Ta spectra for Ta_2O_5, Ta 4f clearly shifted by approximately 0.50 eV toward a lower binding energy when a small amount of Nb was added. The binding energy for the TaO bonding state was approximately 2.4 eV lower than that for Ta_2O_5.[24] Furthermore, a tail state denoted by an asterisk in Figure 3b was observed. In Figure 3b, to compare the shape of the spectra, the spectrum of $(Ta_{0.8}Nb_{0.2})_2O_5$ was offset by +0.5 eV along the *x*-axis. The inset shows a difference peak that is the peak of Ta_2O_5 minus that of $(Ta_{0.8}Nb_{0.2})_2O_5$, which is attributed to the defective state in Ta_2O_5.[25] These results suggested a valence number of 5+ (Ta_2O_5) for Ta and the existence of the defective tail state, which is related to both the oxygen vacancy and the Ta defect. In contrast, with Nb 3d, the changing behavior of the spectral shape was different from that of Ta 4f. The asymmetrical shape became pronounced as the Ta content increased and could be deconvoluted as shown in Figure 3c. The Nb $3d_{5/2}$ spectra at 207.29 and 207.09 eV can be assigned to the Nb_2O_5 and NbO_2 components, indicating that the valence state of Nb was changed by adding Ta.[26,27] In the O1s spectra, the total amount of oxygen increased with increasing Ta content. It can be assumed that the Nb_2O_5 region has a higher oxygen vacancy density than Ta_2O_5. Additionally the valence of Nb 4+ needs less oxygen than the valence of Nb 5+, meaning that the $(Ta_xNb_{1-x})_2O_5$ region should have fewer oxygen vacancies than Nb_2O_5. The oxygen vacancies can be compensated for by controlling the valence of Nb.

Figure 4 shows typical *I*−*V* characteristics for several compositions. The resistance changed when an applied voltage

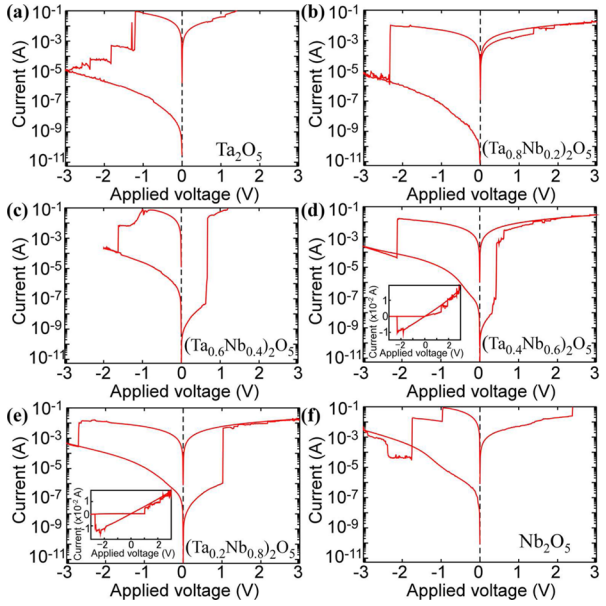

Figure 4. *I*−*V* characteristics of (a) Ta_2O_5, (b) $(Ta_{0.8}Nb_{0.2})_2O_5$, (c) $(Ta_{0.6}Nb_{0.4})_2O_5$, (d) $(Ta_{0.4}Nb_{0.6})_2O_5$, (e) $(Ta_{0.2}Nb_{0.6})_2O_5$, and (f) Nb_2O_5. The current compliance was set at 100 mA.

was swept from a positive bias to a negative bias, indicating that there are two different resistive states in the positive and negative voltage regions; one is a high resistance state (HRS = turn-off) and the other is a low resistance state (LRS = turn-on). With the Ta_2O_5 and Nb_2O_5 regions, the *I*−*V* properties showed poor leakage properties at the initial state, which corresponded to the Ta defect or oxygen vacancy state as observed in the XPS results. Although, the saturation current decreased greatly as a result of the first formation (turn-on and turn-off) process, the turn off process exhibited a step structure as shown in Figure 4a and f. One possible candidate is the Joule heating effect on the oxygen vacancies in the LRS state. Currently, this step structure cannot be controlled, meaning that the oxygen vacancy potentially affects the switching process and makes the formation process unstable. With the composition spread region, and especially the Nb-rich region (Figure 4d and e), the initial leakage properties are better than those of the Ta_2O_5 and Nb_2O_5 regions. The LRS is lower and more stable than the other regions. Furthermore, in the turn-off process, the *I*−*V* property showed a single step structure. The insets in Figure 4d and e show linear plots of the *I*−*V* characteristic, which indicated linearity. Note that the oxygen vacancy model relating to the oxygen migration at the metal/oxide interface shows nonlinear *I*−*V* curves during its formation process,[28,29] meaning that, with Cu/$(Ta_xNb_{1-x})_2O_5$, the majority of the conducting paths at the interface should be metal conducting paths in the oxide (nanoionics model). By combining the XPS and *I*−*V* result, it can be summarized that the $(Ta_xNb_{1-x})_2O_5$ with Nb rich content $(0 < x < 0.5)$ regions with the Cu top electrode is a good candidate for the ReRAM application.

dx.doi.org/10.1021/co4000425 | *ACS Comb. Sci.* 2013, 15, 435−438

CONCLUSIONS

In summary, we have tried using combinatorial synthesis to control the resistive switching properties of the Cu/$(Ta_xNb_{1-x})_2O_5$/Pt structure, whose materials and device structure are compatible with current LSI technology. The as-deposited $(Ta_xNb_{1-x})_2O_5$ film with a grained structure showed resistive switching behavior. XPS revealed that the valence number of Nb and oxygen vacancies were affected by the Ta content. As regards the $I-V$ properties, the valence number of the 5+ region did not exhibit stable resistive changing behavior in contrast to the low Ta content region. In particular, $(Ta_xNb_{1-x})_2O_5$ with a Nb content above 0.5 did not need thermal treatment to obtain initial low leakage current properties, which can reduce the damage caused by the Joule heating effect. These results suggested that doping Nb_2O_5 with Ta makes it possible to control the valence number of Nb and the resistive changing behavior of the Cu/$(Ta_xNb_{1-x})_2O_5$ nano-ionics type ReRAM structure.

AUTHOR INFORMATION

Corresponding Author

*Tel.: +81 29 860 4546. Fax: +81 29 860 4916. E-mail: NAGATA.Takahiro@nims.go.jp.

Notes

The authors declare no competing financial interest.

ACKNOWLEDGMENTS

This work was supported by a Grant-in-aid for Key Technology, "Atomic Switch Programmed Device" from Japan's Ministry of Education, Culture, Sports, Science, and Technology. WPI-MANA was established by World Premier International Research Center Initiative (WPI), the Ministry of Education, Culture, Sports, Science and Technology (MEXT), Japan. The authors would like to acknowledge Ms. Mika Watanabe for technical support with the electrical measurements.

REFERENCES

(1) Waser, R. Resistive non-volatile memory devices. *Microelctron. Eng.* **2009**, *86*, 1925.
(2) Karg, S. F.; Meijer, G. I.; Bednorz, J. G.; Rettner, C. T.; Schtorr, A. G.; Joseph, E. A.; Lam, C. H.; Janousch, M.; Staub, U.; LaMattina, F.; Alvarado, S. F.; Widmer, D.; Stutz, R.; Drechsler, U.; Caimi, D. Transition-metal-oxide-based resistance-change memories. *IBM J. Res. Dev.* **2008**, *52*, 481.
(3) Pagnia, H.; Sotnik, N. Bistable switching in electroformed metal–insulator–metal devices. *Phys. Status Solidi* **1988**, *108*, 11.
(4) Chudnovskii, F. A.; Odynets, L. L.; Pergament, A. L.; Stefanovich, G. B. Electroforming and switching in oxides of transition metals: The role of metal–insulator transition in the switching mechanism. *J. Solid State Chem.* **1996**, *122*, 95.
(5) Asamitsu, A.; Tomioka, Y.; Kuwahara, H.; Tokura, Y. Current switching of resistive states in magnetoresistive manganites. *Nature* **1997**, *388*, 50.
(6) Fors, R.; Khartsev, S. I.; Grishin, A. M. Giant resistance switching in metal–insulator–manganite junctions: Evidence for Mott transition. *Phys. Rev. B* **2005**, *71*, 045305.
(7) Kim, D. S.; Kim, Y. H.; Lee, C. E.; Kim, Y. T. Colossal electroresistance mechanism in a Au/$Pr_{0.7}Ca_{0.3}MnO_3$/Pt sandwich structure: Evidence for a Mott transition. *Phys. Rev. B* **2006**, *74*, 174430.
(8) Meijer, G. I.; Staub, U.; Janousch, M.; Johnson, S. L.; Delley, B.; Neisius, T. Valence states of Cr and the insulator-to-metal transition in Cr-doped $SrTiO_3$. *Phys. Rev. B* **2005**, *72*, 155102.
(9) Waser, R.; Aono, M. Nanoionics-based resistive switching memories. *Nat. Mater.* **2007**, *6*, 833.
(10) Sakamoto, T.; Sunamura, H.; Kawaura, H.; Hasegawa, T.; Nakayama, T.; Aono, M. Nanometer-scale switches using copper sulfide. *Appl. Phys. Lett.* **2003**, *82*, 3032.
(11) Banno, N.; Sakamoto, T.; Hasegawa, T.; Terabe, K.; Aono, M. Effect of ion diffusion on switching voltage of solid-electrolyte nanometer switch. *Jpn. J. Appl. Phys.* **2006**, *45*, 3666.
(12) Terabe, K.; Hasegawa, T.; Nakayama, T.; Aono, M. Quantized conductance atomic switch. *Nature* **2005**, *433*, 47.
(13) Kim, Y.-M.; Lee, J.-S. Reproducible resistance switching characteristics of hafnium oxide-based nonvolatile memory devices. *J. Appl. Phys.* **2008**, *104*, 114115.
(14) Sakamoto, T.; Lister, K.; Banno, N.; Hasegawa, T.; Terabe, K.; Aono, M. Electronic transport in Ta_2O_5 resistive switch. *Appl. Phys. Lett.* **2007**, *91*, 92110.
(15) Lee, S.; Kim, W.-G.; Rhee, S.-W.; Yong, K. Reproducible resistance switching characteristics of hafnium oxide-based nonvolatile memory devices. *J. Electrochem. Soc.* **2008**, *155*, H92.
(16) Gibbons, J. F.; Beadle, W. E. Switching properties of thin NiO films. *Solid-State Electron.* **1964**, *7*, 785.
(17) Tsuchiya, T.; Oyama, Y.; Miyoshi, S.; Yamaguchi, S. Non-stoichiometry-induced carrier modification in gapless type atomic switch device using Cu2S mixed conductor. *Appl. Phys. Express* **2009**, *2*, No. 055002.
(18) Haemori, M.; Nagata, T.; Chikyow, T. Impact of Cu electrode on switching behavior in a Cu/HfO_2/Pt structure and resultant Cu ion diffusion. *Appl. Phys. Express* **2009**, *2*, No. 061401.
(19) Nagata, T.; Haemori, M.; Yamashita, Y.; Iwashita, Y.; Yoshikawa, H.; Kobayashi, K.; Chikyow, T. Oxygen migration at Pt/HfO_2/Pt interface under bias operation. *Appl. Phys. Lett.* **2010**, *97*, No. 082902.
(20) Nagata, T.; Haemori, M.; Yamashita, Y.; Yoshikawa, H.; Iwashita, Y.; Kobayashi, K.; Chikyow, T. Bias application hard X-ray photoelectron spectroscopy study of forming process of Cu/HfO_2/Pt resistive random access memory structure. *Appl. Phys. Lett.* **2011**, *99*, No. 223517.
(21) Ellingham, H. J. T. Reducibility of oxides and sulfides in metallurgical processes. *J. Soc. Chem. Ind., London, Trans. Commun.* **1944**, *63*, 125.
(22) Ahmet, P.; Yoo, Y. Z.; Hasegawa, T.; Koinuma, H.; Chikyow, T. The fabrication of the three components composition spread thin film with controlled composition and thickness. *Appl. Phys. A: Mater. Sci. Process.* **2004**, *79*, 837.
(23) Nagata, T.; Ahmet, P.; Yoo, Y. Z.; Yamada, K.; Tsutui, K.; Wada, Y.; Chikyow, T. Schottky metal library for ZNO-based UV photodiode fabricated by the combinatorial ion beam-assisted deposition. *Appl. Surf. Sci.* **2006**, *252*, 2503.
(24) Kerrec, O.; Devilliers, D.; Groult, H.; Marcus, P. Study of dry and electrogenerated Ta_2O_5 and Ta:Ta_2O_5:Pt structures by XPS. *Mater. Sci. Eng.* **1998**, *B55*, 134.
(25) Kohli, S.; McCurdy, P. R.; Rithner, C. D.; Dorhout, P. K.; Dummer, A. M.; Brizuela, F. C.; Menoni, S. X-ray characterization of oriented β-tantalum films. *Thin Solid Films* **2004**, *469*, 404.
(26) Fontaine, R.; Caillat, R.; Feve, L.; Guittet, M. J. Déplacement chimique ESCA dans la série des oxydes du niobium. *J. Electron Spectrosc. Relat. Phenom.* **1977**, *10*, 349.
(27) Simon, D.; Perrin, C.; Baillif, P. Electron spectrometric study (ESCA) of niobium and its oxides. Application to its oxidation at high temperature and low oxygen pressure. *C. R. Acad. Sci. Ser. C* **1976**, *283*, 241.
(28) Yang, J. J.; Pickett, M. D.; Li, X.; Ohlberg, D. A. A.; Stewart, D. R.; Williams, R. S. Memoristive switching mechanism for metal/oxide/metal nanodevices. *Nat. Nanotechnol.* **2008**, *3*, 429.
(29) Schroeder, H.; Jeong, D. S. Resistive switching in a Pt/TiO_2/Pt thin film stack—A candidate for a non-volatile ReRAM. *Microelectron. Eng.* **2007**, *84*, 1982.